Macromolecules

pubs.acs.org/Macromolecules Article

Decoupling Poly(3-alkylthiophenes)' Backbone and Side-Chain Conformation by Selective Deuteration and Neutron Scattering

Zhiqiang Cao, Zhaofan Li, Song Zhang, Luke Galuska, Tianyu Li, Changwoo Do, Wenjie Xia, Kunlun Hong, and Xiaodan Gu*

Cite This: https://dx.doi.org/10.1021/acs.macromol.0c02086 Read Online

ACCESS | Metrics & More | Article Recommendations | Supporting Information

ABSTRACT: Although considerable progress has been made to optimize the optoelectronic properties of conjugated polymers (CPs), the rational design of CPs with tailored physical properties for end-use applications remains a significant challenge. Specifically, experimental characterization of conjugated polymer backbone conformations remains underexplored due to limited techniques that are capable of distinguishing the backbone and side-chain structures at nanoscopic resolution. Thus, relating the electronically functional backbone conformation to the material's macroscopic optoelectronic property is an ongoing challenge. Here, small-angle neutron scattering techniques (SANS) with contrast-variation (CV) experiments are employed on poly(3-alkylthiophenes) (P3ATs) with both deuterated and protonated side chains in a mixture of protonated and deuterated solvents to decouple the backbone and side-chain scattering signals. We obtained the form factor of P3ATs' backbone, side chains, and cross-scattering term by deconvoluting their respective scattering signals. Poly(3-decylthiophene) shows a persistence length of 1.05 ± 0.1 nm for the conjugated polymer backbone and 2.10 ± 0.2 nm for the entire chain. The strong scattering signal from long and flexible alkyl side chains leads to a seemingly more rigid conjugated polymer, which is further revealed by coarse-grained molecular dynamics (CG-MD) simulations. This work offers a methodology to decouple the scattering contribution from the CPs' backbone and side chains, thus elucidating the inherent conformation of the electronically active conjugated backbone, which provides guidance for the rational design of next-generation polymeric semiconductors.

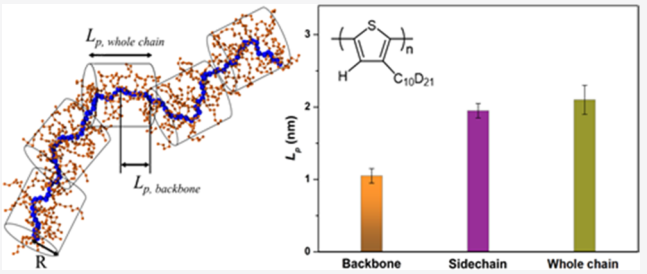

INTRODUCTION

The unique optoelectronic properties and intrinsic mechanical flexibility of conjugated polymers (CPs) are key driving factors for their potential applications in a broad range of devices ranging from organic photovoltaics (OPVs)[1,2] and field-effect transistors (OFETs)[3] to emerging technologies such as thermoelectrics,[4−6] electronic skins,[7−9] stretchable electronics,[10−13] and photodetectors.[14] The chain conformation of CPs affects polymer aggregation and crystallization behavior,[15−21] significantly altering their self-assembled structures,[2,22] mechanical, electronic,[23−25] and optical properties.[26] Interestingly, many CPs used in high-performance OFETs or OPVs were theoretically predicted to be very stiff,[25,26] which highlighted the importance of understanding chain conformation. Despite their essential role, only a few studies have focused on the chain conformation in solution[27−32] and rarely occur in the condensed solid state.

The conjugated backbone directly dictates the optoelectronic properties of the material. Thus, backbone engineering is widely adopted to design new CPs.[33−37] The introduction of more fused rings along the polymer backbone (e.g., indacenodithiophene, diketopyrrolopyrrole, isoindigo, naphthalene diimide moiety) that favor linear and planar conformations was widely adopted. These CPs are generally expected to be relatively stiff. Campoy-Quiles and Nelson et al. suggested that the high optical absorption of CPs originates from their inherently high rigidity.[26] Also, recent coarse-grained (CG) modeling studies demonstrated that the charge diffusion coefficient, a parameter correlated with mobility, rises with increasing chain rigidity as carriers can travel further on an individual chain, provided the chains are sufficiently long.[38] However, the chain conformations of CPs predicted in literature are based on the computational work using density functional theory (DFT) and molecular dynamics (MD) simulations,[39,40] which still require experimental validation. Along this line, de Pablo et al. performed MD simulations and experimental measurements to study the chain conformations of poly({4,8-bis[(2-ethylhexyl)oxy]benzo[1,2-*b*:4,5-*b*′]-dithiophene-2,6-diyl}{3-fluoro-2-[(2-ethylhexyl)carbonyl]-

Received: September 10, 2020
Revised: November 10, 2020

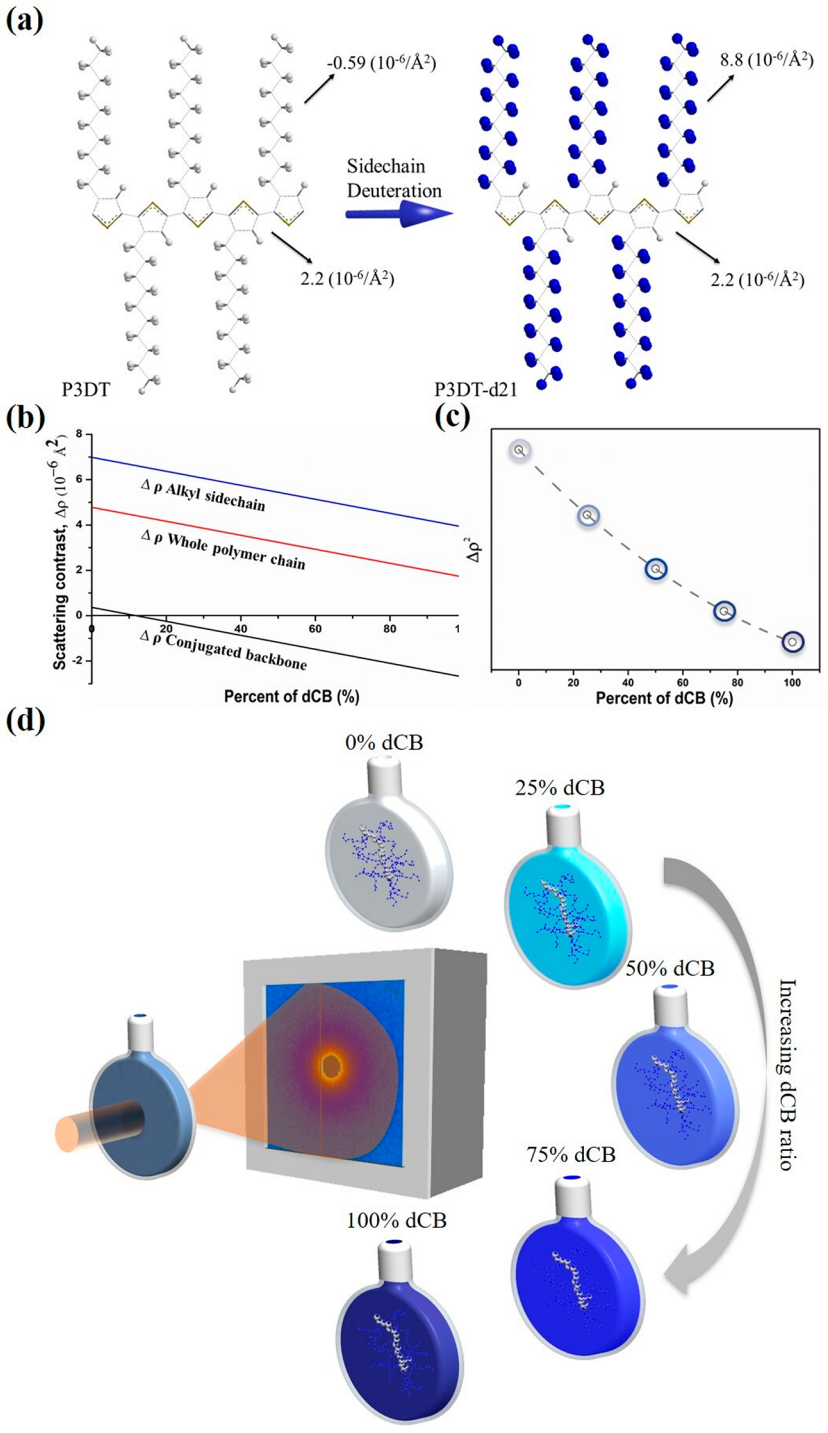

Figure 1. Contrast variation (CV) to highlight the backbone portion of polymer chain. (a) Effect of nonexchangeable deuterium labeling of side chains on the SLD. To calculate the SLD, a density of 1.15 g/cm^3 for P3DT and P3DT-d21 was used. (b) Scattering contrast (the difference in SLD, $\Delta\rho$) between various parts of P3DT-d21 and solvents for different CB:dCB blend ratio. SLD of CB and deuterated chlorobenzene (dCB) are 1.8×10^{-6} and 4.9×10^{-6}/Å^2, respectively. SLD of side chains, backbone, and whole polymer of P3DT-d21 are 8.8×10^{-6}, 2.2×10^{-6}, and 6.6×10^{-6}/Å^2, respectively. (c) Decreases of $\Delta\rho^2$ between whole polymers and solvents with the increasing ratio of dCB in the mixed solvents. (d) Schematic illustration of the use of a series of CV-SANS experiments, with the percentage (vol/vol, dCB:CB) of dCB of 0, 25, 50, 75, and 100%, to tune the SLD of solvents and to decouple the backbone and side-chain conformation. SLD of a solvent matrix, as function of the composition of dCB ratio, is illustrated by the color change.

thieno[3,4-*b*]thiophenediyl}) (PTB7), a well-known CP for photovoltaic application.[31]

Scattering techniques, including light scattering, small-angle X-ray scattering (SAXS), and small-angle neutron scattering (SANS), are widely used for studying single-chain conformations in dilute solution for polymers.[25,41] Light and X-ray scattering, however, are not suitable for quantifying chain rigidity for CPs due to the following reasons. The typical light source (632.8 nm for HeNe laser) from a commonly used light-scattering instrument falls into the band gap of the CPs,

https://dx.doi.org/10.1021/acs.macromol.0c02086
Macromolecules XXXX, XXX, XXX−XXX

causing reduced solution scattering intensity due to polymer absorption, and further trouble the measurements due to potential fluorescence signal from CPs. Both issues create complications in data interpretation and quantification of chain conformation while using light-scattering techniques.[42] Similarly, X-ray scattering has limitations due to strong absorption from the halogenated solvents, commonly used for CPs. For example, low-energy X-ray photons (e.g., 10 000 eV) are strongly absorbed (around 99% for 1 mm beam path) (e.g., chloroform, chlorobenzene (CB) and dichlorobenzene), and very high-energy X-ray source is needed. To measure the chain conformation of CPs dissolved in a halogenated solvent, SANS is a more suitable experimental technique due to the neutron's ability to penetrate samples containing heavy elements. Thus, SANS was commonly used to study the chain conformation of CPs. In general, CPs are relatively rigid. However, depending on the molecular structure of the backbone and the side chains, chain rigidity of CPs which is quantified by persistence length (L_p) can span very large range, from 40 nm for poly(*p*-phenylenevinylene)s (BCHA-PPV)[43] to 1 nm for poly(3-alkylthiophene)s (P3EHT).[27] We encourage readers who are interested to go through Table S1 that summarized the current experimental results of various CPs' L_p. Among various CPs, poly(3-alkylthiophene)s (P3ATs) are the most widely studied so far. Segalman et al. systematically investigated the effect of regioregularity, side-chain chemistry, synthetic route, solvent choice, and temperature on the chain conformation of P3ATs.[44] They found that P3ATs are typical semiflexible polymers with persistence length (L_p) from 1 to 3 nm. Furthermore, Chen et al. found that the branched side-chain structure in P3ATs favors chain conformations that involve twisting of the polymer backbone; thus, they are more flexible when compared to P3ATs with linear side chains.[45] Up to now, previous experiments only consider chain conformation as a whole, from which the entire polymer chain shape was determined. However, CP structures are highly heterogeneous. They have a relatively rigid conjugated backbone that is responsible for their unique optoelectronic properties, while long and flexible insulating alkyl side chains promote the solubility of the polymer in solution. Therefore, the "naked" backbone conformation is especially important in the structure−property relationship for functional semiconducting polymers when correlating chain conformation to the material's macroscopic properties. Taking poly(3-decylthiophene) (P3DT) as an example, since the scattering length density (SLD) for the backbone ($-0.59 \times 10^{-6}/\text{Å}^{-2}$) and side chains ($2.2 \times 10^{-6}/\text{Å}^{-2}$) are similar, it is difficult to characterize the backbone conformation, as shown in Figure 1a.

In this work, we seek to better understand the rigidity of the CP backbone's portion, by decoupling the backbone and side-chain scattering contribution using a combination of contrast-variation neutron scattering and side-chain deuterium labeling. In Figure 1a, deuterium labeling can greatly enhance the SLD of polymers by replacing hydrogen with deuterium. For example, by selective side-chain deuteration, SLD for alkyl side chains raises from $-0.59 \times 10^{-6}/\text{Å}^{-2}$ to $8.8 \times 10^{-6}/\text{Å}^{-2}$, which allows the differentiating of the backbone from side chains. Next, by placing side-chain deuterated P3DT (P3DT-d21) in different contrast-variation (CV) deuterated and hydrogenated solvent mixtures, the contrast factors of various parts of the polymer would be different. Figure 1b shows that the scattering contrast $\Delta\rho$ between whole polymer chain and solvents decreases with the increasing ratio of deuterated chlorobenzene (dCB) in the mixed solvents. Using five CV solvent mixtures with incremental ratios of deuterated solvents, as shown in Figure 1c,d, one can distinguish backbone scattering from side chains.[46−48] In this study, we find lower backbone rigidity compared to the whole polymer chain. The backbone of P3DT exhibited a L_p of 1.05 ± 0.1 nm, while the overall chain showed 2.10 ± 0.2 nm. Complementary to the experimental approaches, coarse-grained molecular dynamics (CG-MD) simulation was conducted to aid our understanding of conformational behaviors of CPs, showing qualitative agreement that the whole polymer chain is more rigid than the conjugated polymer backbone. This work presents the first of its kind to understand the backbone rigidity for CPs and could lead to a better understanding of the role of the conjugated backbone conformation in determining its optoelectronic properties.

METHODS

Synthesis of Side-Chain Deuterated Polymers. Deuterated CP was synthesized using a quasi-living Kumada catalyst transfer polymerization (KCTP) method as reported previously.[49,50] Full synthetic details are described in the Supporting Information. To be specific, we selectively deuterated the side chains of P3DT, as noted as P3DT-d21. Regioregular protonated P3DT was purchased from Sigma-Aldrich.

Size Exclusion Chromatography (SEC). The molecular weights and dispersities of P3DT-d21 and P3DT were measured with a Malvern OMNISEC equipped with OMNISEC RESOLVE and OMNISEC REVEAL. Two PLgel 5 μm mixed-C columns (7.5 mm ID × 300 mm, each) and one PLgel 5 μm guard column (7.5 mm ID × 50 mm) in series were used. Tetrahydrofuran (THF) was used as the eluent (1 mL/min, at 30 °C). Absolute molar masses were calculated which is relative to polystyrene standards.

Nuclear Magnetic Resonance (NMR). ^{1}H NMR and ^{13}C NMR spectra were measured by a Varian-500 MHz NMR spectrometer. Chemical shifts were reported in ppm relative to $CDCl_3$ at 7.27 and 77.23 ppm for ^{1}H NMR and ^{13}C NMR, respectively. ^{1}H NMR was used to confirm the chemical composition of the final product and to calculate the polymer's regioregularity. ^{13}C NMR was also used to calculate the degree of deuteration of P3DT-d21.

Fourier Transform Infrared (FTIR) Spectroscopy. FTIR was recorded in attenuated total reflection (ATR) geometry using a Bruker Optics Vertex 70 spectrometer equipped with a deuterated triglycine sulfate (DTGS) detector. The polymers were loaded to the diamond ATR crystal on a Harrick Scientific MVP 2 Series accessory, and 32 scans at 2 cm^{-1} resolution were collected. A background spectrum (32 scans at 2 cm^{-1} resolution) of the clean ATR crystal was used as the reference. The baseline was corrected by a rubber band correction method using the built-in instrument software package (OPUS).

Differential Scanning Calorimetry (DSC). DSC measurements were performed with a Q-2000 DSC (TA Instruments). The samples were first heated above the melting temperature followed by cooling to −90 °C with a rate of 10 °C/min. After that, the samples were reheated up at the same rate. The DSC data were taken at the cooling and second reheating scan for determining melting temperature and melting enthalpy.

UV−Vis−NIR Spectroscopy. UV−vis−NIR spectra were measured by a Cary 5000 UV−vis−NIR spectrophotometer. Solution absorption data was acquired from dilute solutions of polymer (0.05 mg/mL) in a mixture of deuterated and protonated CB (dCB and CB), with the percentage (vol/vol) of dCB of 0, 25, 50, 75, and 100%.

Small-Angle Neutron Scattering (SANS). To properly perform SANS measurements to probe the conformation of isolated polymer chains, we prepared dilute solutions of polymer (10 mg/mL) in a mixture of dCB and CB, with the percentage (vol/vol) of dCB of 0, 25, 50, 75, and 100%, to tune the SLD of solvents. SANS

https://dx.doi.org/10.1021/acs.macromol.0c02086
Macromolecules XXXX, XXX, XXX−XXX

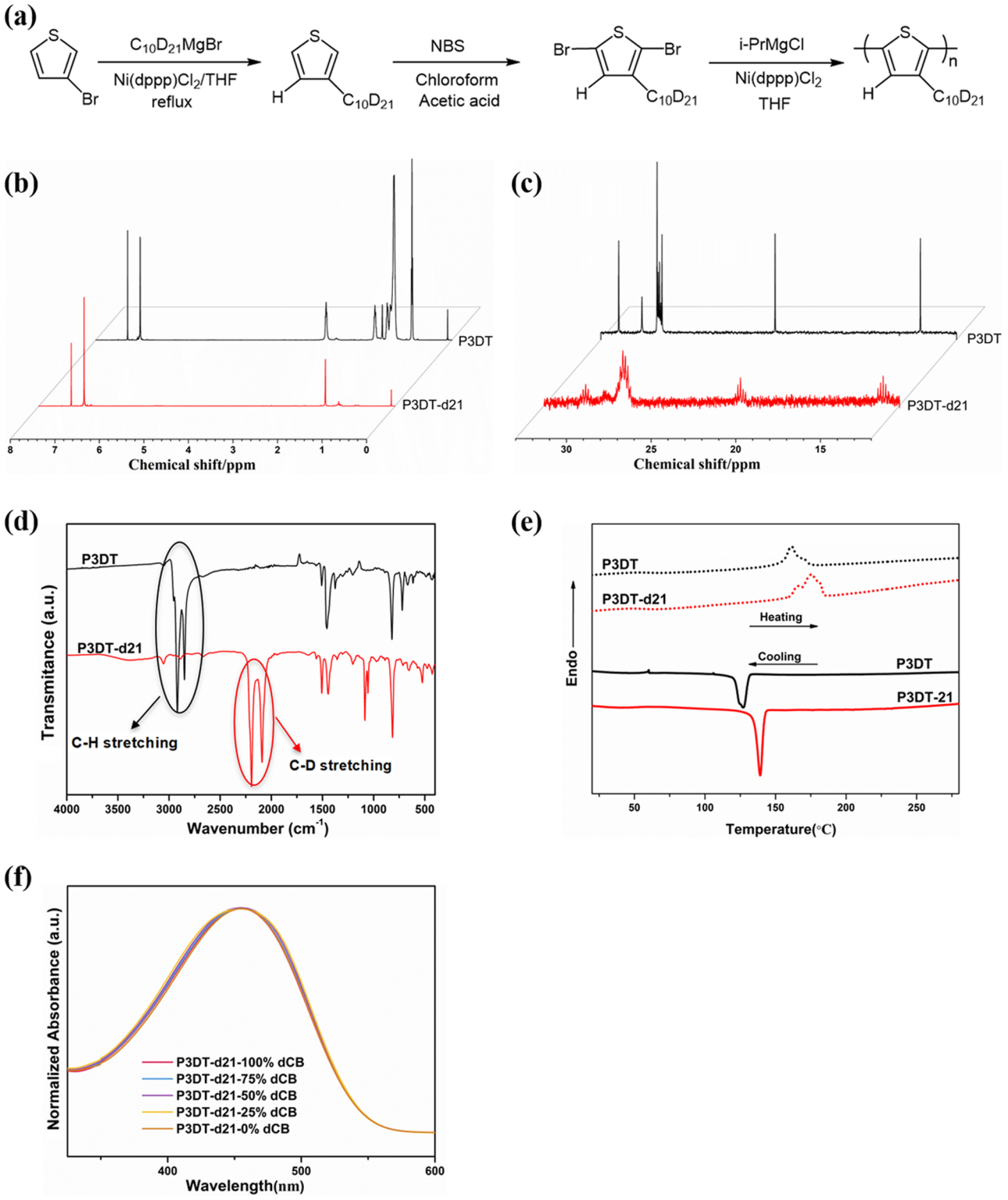

Figure 2. Synthesis of the P3DT polymer with deuterated side chains and its physical property. (a) Synthetic route of poly(3-decylthiophene)-d21. (b) ^{1}H and (c) ^{13}C NMR of P3DT and P3DT-d21. (d) FTIR spectra of P3DT and P3DT-d21. (e) Crystallization and melting behavior for P3DT and P3DT-d21 by DSC (10 °C/min). (f) UV−vis absorption spectra of P3DT-d21 in different contrast-variation solvents (0.05 mg/mL at room temperature).

measurements were carried out using the Extended Q-Range Small-Angle Neutron Scattering Diffractometer (EQ-SANS) at the Spallation Neutron Source (SNS), Oak Ridge National Lab (ORNL) and NG7SANS at National Institute of Standards and Technology (NIST) Center for Neutron Research. The scattering wavevector q ranged from 0.003 to 3 Å^{-1}, using three different configurations (4 m 12 Å, 2.5 m 2.5 Å, and 1.3 m 1 Å). The samples were contained in Hellma quartz cells with a 2 mm path length. Solution SANS measurements were performed at 75 °C. Data reduction and correction to get absolute intensity were performed. The data were put on an absolute scale by introducing the differential cross-section per unit volume of porasil (cm^{-1}).

https://dx.doi.org/10.1021/acs.macromol.0c02086
Macromolecules XXXX, XXX, XXX−XXX

Table 1. Number Averaged Molecular Weight (M_n), Dispersity ($Đ$), Regioregularity, Degree of Deuteration of Side Chains, Melting Temperature, and Melting Enthalpy of P3AT Polymers

polymer	M_n (kDa)	$Đ$	regioregularity (%)	degree of deuteration (%)	T_m (°C)	ΔH_m (J/g)
P3DT	45.4	1.63	95	0	161.3	10.8
P3DT-d21	20.6	1.07	97	99	175.7	15.2

Overview of CG-MD Simulations. In addition to the experiments, CG-MD simulations are performed to further achieve a more visualizing understanding of how backbone conformation differs from whole polymer chain conformation. We describe the polymer backbone and side chains based upon a bead-spring CG model as a set of connected beads.[51,52] The backbone is composed of $N_b = 100$ segments, and the side chains each composed of $N_{sc} = 10$ segments. Nonbonded pair interactions between all types of beads are modeled by a cut-and-shifted Lennard-Jones (LJ) potential[53,54]

$$U_{LJ}(r) = \begin{cases} 4\varepsilon\left[\left(\frac{\sigma}{r}\right)^{12} - \left(\frac{\sigma}{r}\right)^{6} + \frac{1}{4}\right], & r < 2^{1/6}\sigma \\ 0, & r \geq 2^{1/6}\sigma \end{cases} \quad (1)$$

where ε and σ refer to the units of LJ energy and length, and the distance between two beads is denoted by r. This choice of LJ potential ensures U_{LJ} altering continuously to zero and results in purely repulsive interactions between segments to mimic the solution state in a good solvent. For bonded beads along the chain additionally, the stiff harmonic spring is used, $U_{bond}(r) = k_b(r - r_0)^2$, where $r_0 = 0.97\sigma$ is the equilibrium bond length and $k_b = 2500\varepsilon/\sigma^2$ is the spring constant, consistent with the previous branched polymer studies.[55,56] Moreover, chain stiffness is controlled by utilizing a three-body angular potential, $U_{angle}(\theta) = k_\theta(1 + \cos(\theta))$, where angular stiffness constant k_θ is set as 0.7ε and 0.2ε to control the stiffness of backbone and side chains, respectively. All quantities and results in CG modeling are expressed in standard reduced LJ units by the properties of the polymer. It should be noted that these forcefield parameters are implemented to qualitatively describe the approximate molecular structure informed from the experimentally studied CP in solution.

Large-scale atomic/molecular massively parallel simulator (LAMMPS) simulation package is applied to perform all CG-MD simulations,[57] and the visualization of CP snapshots is performed through the visual molecular dynamics (VMD).[58] Periodic boundary conditions are applied in all directions and an integration timestep of $\Delta t = 0.002\tau$ is adopted, where τ is given in unit $\sigma(m/\varepsilon)^{1/2}$. To equilibrate the system, the energy minimization is first performed using the iterative conjugate gradient algorithm, followed by dynamics equilibration runs at temperature $T = 0.6$ in reduced unit under the canonical (NVT) ensemble and continued up to 1×10^7 time steps. Equilibration and structural stability are confirmed by monitoring the total potential energy that saturates to a nearly constant value at the end of the equilibration process.

RESULTS AND DISCUSSION

Synthesis of Deuterated Conjugated Polymers. To perform the CV experiment, we first synthesized P3DT-d21 polymers by a quasi-living Kumada catalyst transfer polymerization (KCTP) method according to previous reports (see the Supporting Information). The synthetic route is shown in Figure 2a. The molecular weight and dispersity of synthesized P3DT-d21 and commercially available P3DT polymers were characterized by SEC using THF as eluent at 30 °C. Table 1 summarized the molecular weights and dispersity of the two polymers.

^{1}H NMR and ^{13}C NMR spectroscopy were utilized to confirm the success of the deuteration of P3DT-d21. For P3DT-d21, the peaks ascribed to H of alkyl side chains disappeared, from ^{1}H NMR spectra (Figure 2b). For P3DT, clear proton peaks were found at the following locations: $CDCl_3$, δ (ppm) = 2.81 (t, 2H), 1.71 (m, 2H), 1.43 (m, 2H), 1.37 (m, 2H), 1.29 (m, 10H), 0.88 (t, 3H). Also, as seen in the ^{13}C NMR spectra (Figure 2c), for P3DT-d21, a septet was observed for CD_3, and the quintet was observed at all CD_2 unit positions due to the spin−spin couplings between ^{13}C and D atoms, rather than a single peak for all of the carbons in the side chains of P3DT.[59] The degree of deuteration of each CD_2 and CD_3 unit is over 99% according to the integrated area of the peaks of fully deuterated CD_2 and CD_3 and partially deuterated CD_2 and CD_3. The degree of side-chain deuteriation could influence the contrast factors. However, this is not the case here. In this work, side chains were nearly fully deuteriated. The effect of labeling distribution on contrast factors due to deuteriation defects is negligible.

Additionally, the successful synthesis of P3DT-d21 was confirmed by the Fourier transform infrared (FTIR) spectra (Figure 2c), showing large shift from low-energy peak 2950−2850 cm^{-1} to high-energy peak 2300−2000 cm^{-1}. Strong absorption bands of P3DT at 2950−2850 cm^{-1} can be attributed to the asymmetric C−H stretching vibrations in $-CH_3$, $-CH_2$ and the symmetric C−H stretching vibration in $-CH_2$, respectively.[60,61] Once the polymer is deuterated, the asymmetric C−D stretching vibrations in $-CD_3$, $-CD_2$ and the symmetric C−D stretching vibration in $-CD_2$ shifted to 2300−2000 cm^{-1}, by a factor of $(m_H/m_D)^{1/2}$ (m_H and m_D denote the atomic masses of H and D, respectively).[61] Its lack of C−H stretching bands also confirms its near full deuteration for P3DT-d21. We observed that the melting point and melting enthalpy of P3DT-d21 increased by 14.4 °C and 4.4 J/g compared with P3DT (Figure 2d and Table 1) because of the relatively lower molecular weight (20.6 vs 45.4 kDa) as well as a slightly higher regioregularity (97 vs 95%).

The ultraviolet−visible (UV−vis) absorption spectra of all P3DT-d21 in different CV solvents were measured. Polymer conjugation length is expected to directly correlate to optical absorption shifts based on previous studies of conjugated oligomers.[62−64] The L_p of the chain has been believed to be an upper limit for the conjugation length. It is clearly shown in Figure 2f that at all different contrast-variation solvents, P3DT-d21 has similar absorption spectra with a maximum centered ∼460 nm. The results suggest that the chain conformation of P3DT-d21 is consistent in different CV solvents. In this work, we assumed that the isotopic exchange H−D does not greatly affect the thermodynamics of the system and the electronic state of the monomers.[47] Thus, the same interactions are involved in P3DT and P3DT-d21 at different CV solvents.

Contrast-Variation Small-Angle Neutron Scattering. We then performed CV-SANS measurements for P3DT-d21 in various CB and dCB solvent mixtures. To achieve enough signal-to-noise ratio, a more concentrated polymer solution is preferred for achieving a stronger scattering signal due to increased scattering sites. Meantime, the chains should not overlap or interact with each other, to ensure that the scattering data is representative for the form factor of an

https://dx.doi.org/10.1021/acs.macromol.0c02086
Macromolecules XXXX, XXX, XXX−XXX

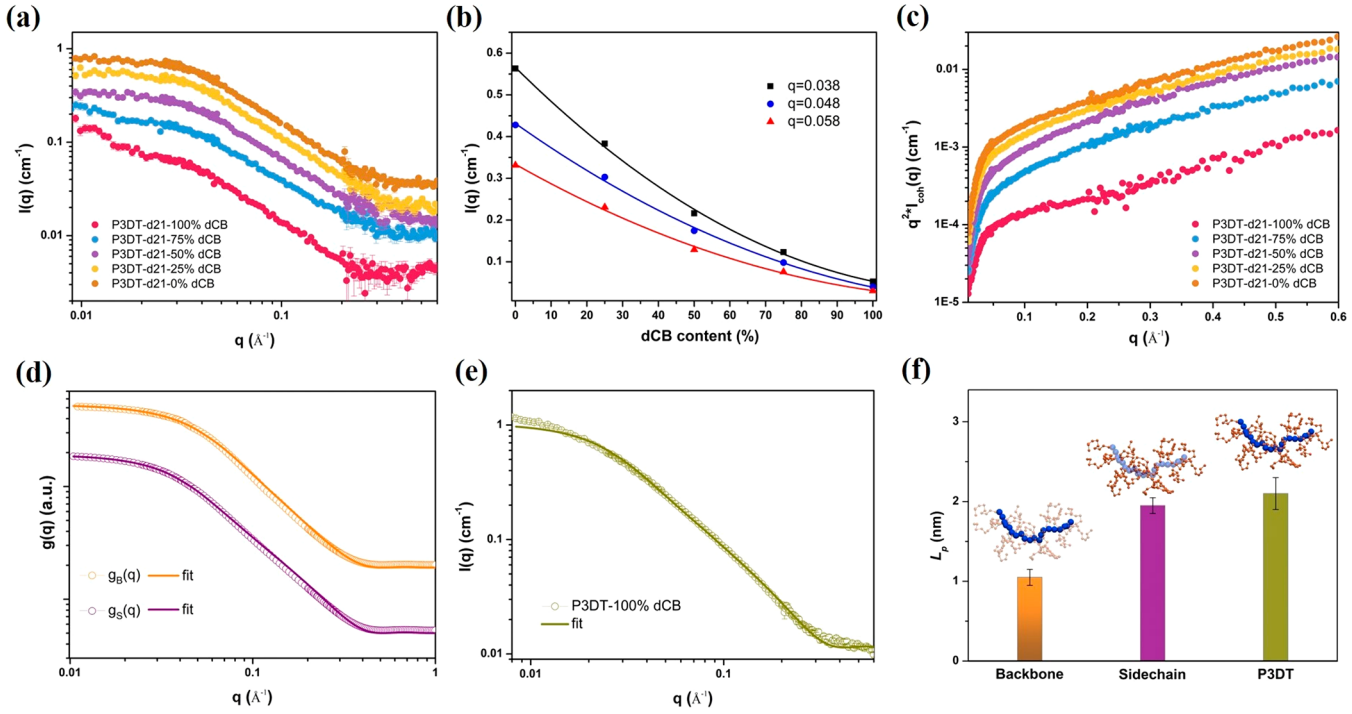

Figure 3. Contrast-variation scattering experiment to probe backbone conformation. (a) Scattering profiles for P3DT-d21 from five different CV conditions at a concentration of 10 mg/mL at 75 °C. (b) $I(q)$ decreases with dCB composition at fixed q. Solid lines correspond to the best fits using parabola functions. (c) Kratky plots for P3DT-d21 in different CV experiments. (d) Form factors $g_B(q)$ for backbone portion and $g_S(q)$ for side-chain portion after deconvolution using eq 8. Solid lines correspond to the best fit to the flexible cylinder model. (e) SANS data for P3DT in dCB (10 mg/mL). The solid line corresponds to the best fit to the flexible cylinder model. (f) L_p of backbone, side chain, and P3DT obtained from fitting to correlation functions $g_B(q)$, $g_S(q)$ of P3DT-d21 and SANS data for P3DT in 100% dCB with the flexible cylinder model. For backbone L_p, side chains are semitransparent for clarity. For side-chain L_p, backbones are semitransparent for clarity.

isolated dissolved chain. SANS can be used to characterize the radius of gyration (R_g) and then determine the critical overlap concentration (C^*), above which interchain interactions are significant. According to Doi, C^* can be calculated by the following equation

$$C^* = \frac{M_n}{N_A \cdot (4/3\pi \cdot R_g^3)} \quad (2)$$

where M_n is the number averaged molecular weight (Table 1) and N_A is Avogadro's number.[65] R_g can be determined by fitting SANS data using the Gauss coil model embedded in SasView. R_g of for P3DT-d21 used in this work was determined to be 3.6 and 7.2 nm for P3DT. Thus, C^* were calculated to be 105.4 and 29.1 mg/mL, respectively, for P3DT-d21 and P3DT in chlorobenzene. This analysis rationalizes the use of a 10 mg/mL concentration to study the conformation of dilute P3DT-d21 and P3DT in solution in this work. Intermolecular correlations are negligible in this case or the structure factor is constant at all q range and equal to 1.

Representative SANS curves of P3DT-d21 for different CV experiments are shown in Figure 3a. For all different CV experiments, the scattering intensity of P3DT-d21 is dominated by the −1.1 to −1.3 decay over the medium q range between 0.05 and 0.1 Å^{-1} and reach Guinier region at even lower q range. This indicated that P3DT-d21 should be approximated by semiflexible chains. One-dimensional rodlike objects have a $I - q$ dependence of −1 in the double log presentation, while a Gaussian coil would show scattering intensity scales as q^{-2}.[27] Semiflexible chains's scattering profile in the intermediate scattering region are expected to have a slope between −1 and −2. Not surprisingly, under different CV conditions, scattering profiles did not differ, but intensities showed drastic differences due to changes in contrast, as shown in Figure 3a. In this example, $\Delta\rho$ between whole polymers and solvents decreases with the increasing ratio of dCB in the mixed solvents. Thus, Figure 3b depicts the typical parabolic $I(q)$ dependence on dCB composition at fixed q. Consistent with the calculated results as shown in Figure 1c, all five different solvent conditions did not reach the contrast match point for whole polymers since $I(q)$ did not fully vanish.

In addition, it is worth noting that an upturn in scattering at low q (below 0.012 Å^{-1}) was shown for P3DT-d21-100% and P3DT-d21-75% dCB. This is likely due to a small fraction of P3DT-d21 aggregating in solution because of strong intermolecular interactions.[66] In this case, we avoided these regions and used an appropriate q range (0.012 Å^{-1} to 0.6 Å) to decouple backbone and side-chain chain conformation. We also performed CV-SANS measurements for side-chain deuterated poly(3-hexylthiophene) (P3HT-d13) in various CB and dCB solvent mixtures at 5 mg/mL with SANS curves shown in Figure S7. At this concentration, we still have not been able to avoid the formation of aggregates. An upturn in scattering at low q region (below 0.03 Å^{-1}) was shown for P3HT-d13-100% and P3HT-d13-75% dCB, indicating the formation of aggregates. We could not find three CV curves (only one curve is not enough), which have shown Guinier region signaled by scattering intensity plateau to decouple the backbone and side-chain scattering. Thus in this work, we will focus the discussion on P3DT-d21 polymer. Before we perform a quantitative analysis of polymer conformation, it is

https://dx.doi.org/10.1021/acs.macromol.0c02086
Macromolecules XXXX, XXX, XXX−XXX

intuitive to investigate the qualitative features of the SANS data by Kratky plots.[45] Kratky plots can qualitatively assess the flexibility of polymers. Figure 3c shows that P3DT-d21 are semiflexible chains as revealed by the high-q upturn in the experimental results that deviate from the predicted plateau of the Debye model for flexible polymer chains.

We consider the P3DT-d21 polymer as a complex with two components: backbone and side chains. Thus, for different CV conditions, the scattering contribution of backbone, side chains, and the cross term between backbone and side chains to the scattering of the chain can vary significantly due to changes in contrast. In this study, the SANS absolute intensity (I) of the dissolved polymers follows by the following expression

$$I = I_{coh} + I_{inc} \tag{3}$$

where I_{coh} is the coherent scattering intensity and I_{inc} is the incoherent scattering intensity, which is independent of q. The small incoherent background due to the presence of the protonated polymer backbone can be disregarded in good approximation. The coherent scattering intensity of one single chain is following

$$I_{coh} = K^2 S(q) \tag{4}$$

where K (cm^{-2}) is the contrast factor between the polymer and the solvent and $S(q)$ is the chain form factor per unit volume (cm^{-3}).

$$K = v(\rho - \rho_{sol}) \tag{5}$$

where ρ is the SLD of the monomers of volume v and ρ_{sol} is that of the solvent.

For CP as a complex with two components: the backbone referred to as symbol "B" and the side chains referred to as symbol "S"; three correlation functions have to be considered: S_B for the backbone, S_S for the side chains, and the cross term S_{BS}. Equation 4 is then replaced by

$$I_{coh} = K_B^2 S_B(q) + K_S^2 S_S(q) + 2K_B K_S S_{BS}(q) \tag{6}$$

with

$$K_B = v_B(\rho_B - \rho_{sol}) \quad K_S = v_S(\rho_S - \rho_{sol})$$

where ρ_B and ρ_S are the SLD of the backbone and side chains of the monomer of volumes v_B and v_S, respectively.

Pair correlations between monomers within the polymer chain are what we want to observe, and the corresponding dimensionless form factor $g(q)$ is defined as

$$g(q) = (m/cN_A)S(q) \tag{7}$$

where m is the molar mass of monomers (g mol^{-1}), c is the concentration of the polymer (g/cm^{-3}), and N_A is the Avogadro's number (mol^{-1}).[47] Equation 4 is then replaced by

$$\frac{m}{cN_A} I_{coh} = K_B^2 g_B(q) + K_S^2 g_S(q) + 2K_B K_S g_{BS}(q) \tag{8}$$

To obtain the three form factors: $g_B(q)$ for the backbone, $g_S(q)$ for side chains, and the cross term $g_{BS}(q)$, three CV conditions where three independent relations are needed, as the intermolecular correlations, structure factor, were neglected for a dilute solution. For different CV conditions, the values of the contrast factors are calculated and listed in Table 2. In this work, five CV conditions with adjusted SLD of the solvent are implemented using a mixture of deuterated and protonated solvent. The contributions of g_B, g_S, and g_{BS} to the form factor of the chain are governed by the ratios K_B^2/K^2, K_S^2/K^2, and $2K_BK_S/K^2$, respectively.

Table 2. Neutron Scattering Contrast Factors for P3DT-d21 in Different Solvents

contrast factor (10^{-24} cm^2)	P3DT-d21-0% dCB	P3DT-d21-25% dCB	P3DT-d21-50% dCB	P3DT-d21-75% dCB	P3DT-d21-100% dCB
K^2	17.29	12.17	7.94	4.61	2.18
K_B^2	0.011	0.014	0.16	0.32	0.62
K_S^2	16.43	13.01	9.98	7.35	5.22
$2K_BK_S$	0.86	−0.84	−2.15	−3.07	−3.58

Using the coherent differential cross sections for the three CV conditions (fitted data using a flexible cylinder model embedded in SasView of P3DT-d21-0% dCB, P3DT-21-50% dCB, P3DT-d21-75% dCB) obtained from dilute solutions and solving eq 8, we have got the form factor $g_B(q)$, $g_S(q)$. The results are presented in Figure 3d. At low q region, a constant plateau for both $g_B(q)$ and $g_S(q)$ is shown below q = 0.02 $Å^{-1}$. For this low q region corresponding to a spatial scale much larger than the polymer coil size, the chain is approximated by a Gaussian coil and a constant plateau is shown in this region. From an experimental point of view, below this value, universal models that do not depend on features of the monomer species, such as Debye function, can be used to describe an experimental scattering curve. On a shorter spatial scale comparable with the length of a few monomers, the universal descriptions are no longer applicable, and we must take into account the local rigidity of the chain. The shapes of scattering functions, $g_B(q)$, $g_S(q)$ are found to be quite different beyond q = 0.02 $Å^{-1}$, as shown in Figure S9. The form factors $g_B(q)$ and $g_S(q)$ obtained at larger q values reflect the local rigidity of the chain and differ from each other.

After the form factors of the backbone and side chains were obtained, the L_p of the naked backbone and side chains could be acquired by fitting the form factors $g_B(q)$ and $g_S(q)$ using a flexible cylinder model in SasView.[31,67] The best fit for the flexible cylinder model and parameters obtained from fits to the flexible cylinder model are shown in Figure 3d and Table S3. One can extract chain conformation, such as contour length, persistence length (L_p), and cylinder radius. The contour length for P3DT-d21 was determined to be 20.03 ± 0.5 nm, which is in a reasonable agreement with the molecular weight, 20.6 kDa, characterized by SEC. The L_p of P3DT-d21's naked backbone and side chains is shown in Figure 3f. The naked backbone of P3DT-d21 has a significantly lower L_p as compared to the apparent L_p of the chain neglecting backbone contribution, at 1.05 ± 0.1 versus 1.95 ± 0.1 nm. Also, we performed SANS on protonated P3DT in dCB. The best fit for the flexible cylinder model, where the L_p of the whole polymer chain was obtained from the scattering contribution of both backbone and side chains, and parameters obtained from fits to the flexible cylinder model are shown in Figure 3e and Table S3. P3DT shows a whole polymer chain L_p of 2.10 ± 0.2 nm. Thus, the naked backbone L_p of P3DT-d21 differs greatly from that of the whole polymer chain, at 1.05 ± 0.1 versus 2.10 ± 0.2 nm. We also used the WORM+Chains (RW)_Rc model embedded in SASfit[68,69] to fit our data to get the whole chain conformation, and the results agree well with the results from the flexible cylinder model (Figure S9 and Table S3). The acquired L_p of the entire polymer is consistent with the chain rigidity for nondeuterated P3ATs determined by Segalman et

https://dx.doi.org/10.1021/acs.macromol.0c02086
Macromolecules XXXX, XXX, XXX−XXX

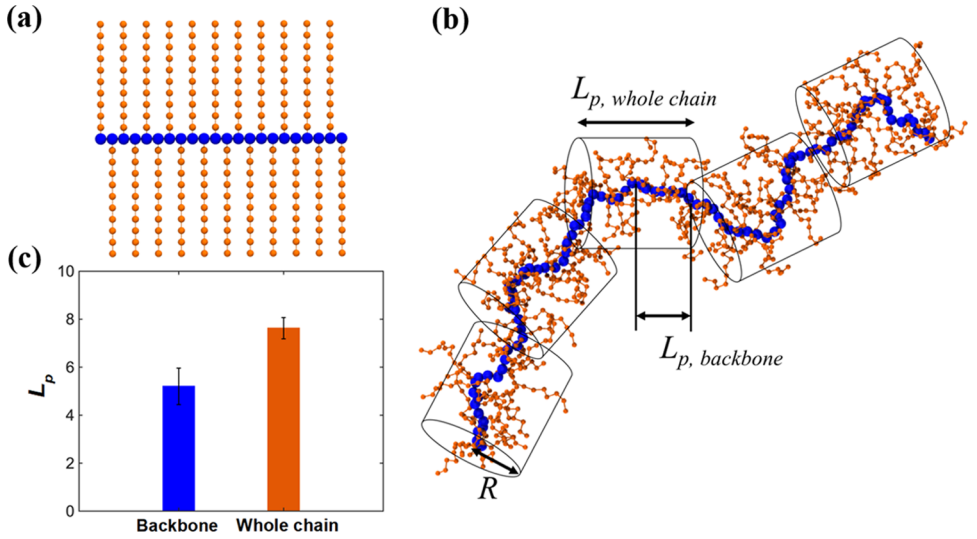

Figure 4. CG-MD simulation of chain confirmation for the P3DT polymer model. (a) Representative architecture of a simulated CP consisting of a backbone composed of N_b = 100 segments (blue beads) and the side chains each composed of N_{sc} = 10 segments (orange beads). (b) Snapshot of a CP simulated using the CG model in a solution state, where schematic cylinders denote a chain of effective persistence segments of length $L_{p,whole\ chain}$ and cross-sectional radius of R. (c) Comparison of the L_p of backbone and the center of geometry (COG) of multiple pairs of side chains, which are calculated through the integral definition of L_p shown in eq 9. The L_p value is in reduced LJ units.

al. They found P3DDT with dodecyl side chains has a L_p of 1 nm, and the L_p of P3HT with hexyl side chains is 3 nm.[44] Similarly, Pozzo et al. found P3DDT and P3HT have a L_p of 3 nm.[30]

CG-MD Simulations. We performed CG-MD simulation to aid our understanding for the chain conformational behaviors by employing a CG model informed from P3DT as shown in Figure 4a, where backbone and side chains are represented by blue and orange beads, respectively. For P3DT having a relatively larger side-chain length, side chains tend to be stretched due to the steric hindrance of neighbor side chains, which can be clearly observed from our CG-MD simulations. Figure 4b shows a simulation snapshot of the CG model of P3DT in a vacuum simulation cell to mimic a solution state, suggesting that the overall contour of the P3DT considering both the backbone and side chain would appear more rigid than polymer backbone only. While it is intuitive to observe that backbone conformation differs greatly from the whole chain conformation, separating the prediction of L_p of the backbone from the side chains for the CPs is still challenging in simulations. Typically, L_p can be defined in simulations in terms of the decay of the orientational correlations of the backbone tangents or/and the average projection of the end-to-end vector of the polymer chain onto the unit backbone vector.[70−74] However, this approach does not explicitly take the side-chain conformation into account for characterizing the chain rigidity of CPs. Despite different proposed approaches,[70,75] there is currently no consensus regarding the most accurate estimate for L_p when relatively large side chains cannot be ignored.

In this CG-MD simulations, we apply the integral function to quantify the geometrical L_p by the following equation to avoid potential shortcoming in view of the decay-fitting difficulties[63,66]

$$L_p = l_b \sum_{s=1}^{N_b-1} \langle \cos\theta(s) \rangle \approx l_b \int_0^{N_b-1} \langle \cos\theta(s) \rangle \, ds \quad (9)$$

where $\langle \cos\theta(s) \rangle$ refers to the directional correlation between two segments and the angular bracket includes an average over multiple trajectories of the dynamics run. This L_p definition has been recently adopted in the study of bottlebrush polymer.[66] To interpret the contributions of the side chains to L_p, the center of geometry (COG) assumption—that center of geometry of a pair of side chains connecting with two adjacent backbone segments as a pseudo-chain further subsequently forming an effective pseudo-chain—is utilized to estimate the L_p of overall contour of the CP. Here, five different simulations with independent initial configurations are used to obtain the average value of L_p, and the error bars correspond to standard deviations. Figure 4c shows the results of L_p estimate for considering backbone only and effective pseudo-chain consisting of COG of multiple pairs of side chains, respectively. The L_p of the backbone is observed to be much smaller than that of the whole chain contour from our simulations, which shows a qualitative agreement with our experimental observations as shown in Figure 3f. It should be mentioned that this COG assumption may still underestimate the L_p of overall contour due to a lack of more detailed description of each side-chain conformation and size, which are difficult to be accurately captured, but is evidenced to better describe the L_p of the whole CP compared to the previous approaches that only account for backbone chain conformation.

CONCLUSIONS

To understand the heterogeneous structure of CPs, decoupled backbone and side-chain conformations in CPs were achieved by the combination of neutron scattering and deuterium labeling. Both experimental and computational results show that the backbone of P3DT-d21 has a significantly lower L_p as compared to the whole polymer chain. The strong scattering signal from long side chains leads to an increased rigidity for the whole polymer chain compared to its backbone. Conventional solution SANS scattering using CPs in deuterated solvent would have scattering signal dominated by the high scattering contrast from the side chain/solvent rather than

https://dx.doi.org/10.1021/acs.macromol.0c02086
Macromolecules XXXX, XXX, XXX−XXX

backbone in which the whole polymer chain conformation is determined. Previous studies might overestimate the backbone rigidity of the CP using scattering techniques, as conformation of the electronically active polymer backbone directly determines the optoelectronic properties of CPs. This work highlights the need for neutron scattering and deuterium labeling to further understand the CPs' backbone conformation and provides a pathway to link the backbone conformation to the CP's optoelectronic properties.

Furthermore, extracting the backbone rigidity for high performance but apparently disordered donor−acceptor (D−A) CPs will also benefit the understanding of the origin of the high performance, for which the rigid backbone has been commonly believed to be the origin of high performance.[76] We also anticipate broader research impacts from this work on a wide range of materials, including comblike and bottlebrush polymers. There still remains a matter of debate in the scientific literature on the interplay between side extension in the comblike and bottlebrush polymers and their impact on chain conformations. Significantly less attention has been paid to the structural heterogeneity of these materials. Our methodology and modeling framework could provide a pathway to address those fundamental problems.

■ ASSOCIATED CONTENT

Supporting Information

The Supporting Information is available free of charge at https://pubs.acs.org/doi/10.1021/acs.macromol.0c02086.

Full synthetic details and SANS profiles and fitting parameters; ^{1}H NMR spectra of 3-decylthiophene-d21 (Figure S1); ^{13}C NMR spectra of 3-decylthiophene-d21 (Figure S2); ^{1}H NMR spectra of 2,5-dibromo-3-decylthiophene-d21 (Figure S3); ^{13}C NMR spectra of 2,5-dibromo-3-decylthiophene-d21 (Figure S4); GPC curves (Figure S5); SANS data for five mixtures of deuterated and protonated chlorobenzene (Figure S6); SANS absolute intensity I(q) (Figure S7); SANS data for P3DT-d21 (Figure S8); Normalized form factor (Figure S9); SANS data for P3DT-d21 in different CV conditions (Figure S10); persistence lengths of common conjugated polymers (Table S1); parameters obtained from fits to SANS data (Table S2); parameters obtained from fits to correlation functions (Table S3); parameters obtained from fits to SANS data (Table S4) (PDF)

■ AUTHOR INFORMATION

Corresponding Author

Xiaodan Gu − *School of Polymer Science and Engineering, The University of Southern Mississippi, Hattiesburg, Mississippi 39406, United States;* orcid.org/0000-0002-1123-3673; Email: xiaodan.gu@usm.edu

Authors

Zhiqiang Cao − *School of Polymer Science and Engineering, The University of Southern Mississippi, Hattiesburg, Mississippi 39406, United States*

Zhaofan Li − *Department of Civil and Environmental Engineering, North Dakota State University, Fargo, North Dakota 58108, United States*

Song Zhang − *School of Polymer Science and Engineering, The University of Southern Mississippi, Hattiesburg, Mississippi 39406, United States;* orcid.org/0000-0001-9815-7046

Luke Galuska − *School of Polymer Science and Engineering, The University of Southern Mississippi, Hattiesburg, Mississippi 39406, United States*

Tianyu Li − *Center for Nanophase Materials Sciences, Oak Ridge National Laboratory, Oak Ridge, Tennessee 37831, United States; Department of Materials Science and Engineering, University of Tennessee, Knoxville, Tennessee 37996, United States;* orcid.org/0000-0003-2324-6452

Changwoo Do − *Neutron Scattering Division, Oak Ridge National Laboratory, Oak Ridge, Tennessee 37831, United States;* orcid.org/0000-0001-8358-8417

Wenjie Xia − *Department of Civil and Environmental Engineering, North Dakota State University, Fargo, North Dakota 58108, United States;* orcid.org/0000-0001-7870-0128

Kunlun Hong − *Center for Nanophase Materials Sciences, Oak Ridge National Laboratory, Oak Ridge, Tennessee 37831, United States;* orcid.org/0000-0002-2852-5111

Complete contact information is available at: https://pubs.acs.org/10.1021/acs.macromol.0c02086

Notes

The authors declare no competing financial interest.

■ ACKNOWLEDGMENTS

This work was supported by the U.S. Department of Energy, Office of Science, Office of Basic Energy Science under award number of DE-SC0019361. L.G. acknowledges partial traineeship support from the NSF NRT program (DEG #1449999). Z.L. and W.X. acknowledge the support from the North Dakota Established Program to Stimulate Competitive Research (ND EPSCoR) through the New Faculty Award. Part of the research used resources at the Spallation Neutron Source and the Center for Nanophase Materials Sciences, DOE Office of Science User Facilities operated by the Oak Ridge National Laboratory. SANS measurements were carried out using the EQ-SANS at SNS, ORNL, and SANS at NIST Center for Neutron Research. Supercomputing support from CCAST Thunder HPC System at NDSU is acknowledged. The authors thank Peter V. Bonnesen (CNMS) for assistance during the NMR experiments. We thank Dr. Yun Liu for assisting sample measurements at NIST and helpful discussion.

■ REFERENCES

(1) Heeger, A. J. 25th Anniversary Article: Bulk Heterojunction Solar Cells: Understanding the Mechanism of Operation. *Adv. Mater.* **2014**, *26*, 10−28.

(2) Liu, Y.; Zhao, J.; Li, Z.; Mu, C.; Ma, W.; Hu, H.; Jiang, K.; Lin, H.; Ade, H.; Yan, H. Aggregation and Morphology Control Enables Multiple Cases of High-Efficiency Polymer Solar Cells. *Nat. Commun.* **2014**, *5*, No. 5293.

(3) Sirringhaus, H. 25th Anniversary Article: Organic Field-Effect Transistors: The Path Beyond Amorphous Silicon. *Adv. Mater.* **2014**, *26*, 1319−1335.

(4) Petsagkourakis, I.; Tybrandt, K.; Crispin, X.; Ohkubo, I.; Satoh, N.; Mori, T. Thermoelectric Materials and Applications for Energy Harvesting Power Generation. *Sci. Technol. Adv. Mater.* **2018**, *19*, 836−862.

(5) Russ, B.; Glaudell, A.; Urban, J. J.; Chabinyc, M. L.; Segalman, R. A. Organic Thermoelectric Materials for Energy Harvesting and Temperature Control. *Nat. Rev. Mater.* **2016**, *1*, No. 16050.

(6) Thomas, E. M.; Popere, B. C.; Fang, H.; Chabinyc, M. L.; Segalman, R. A. Role of Disorder Induced by Doping on the

Thermoelectric Properties of Semiconducting Polymers. *Chem. Mater.* **2018**, *30*, 2965−2972.
(7) Hammock, M. L.; Chortos, A.; Tee, B. C.-K.; Tok, J. B.-H.; Bao, Z. 25th Anniversary Article: The Evolution of Electronic Skin (E-Skin): A Brief History, Design Considerations, and Recent Progress. *Adv. Mater.* **2013**, *25*, 5997−6038.
(8) Wang, S.; Oh, J. Y.; Xu, J.; Tran, H.; Bao, Z. Skin-Inspired Electronics: An Emerging Paradigm. *Acc. Chem. Res.* **2018**, *51*, 1033−1045.
(9) Wang, S.; Xu, J.; Wang, W.; Wang, G.-J. N.; Rastak, R.; Molina-Lopez, F.; Chung, J. W.; Niu, S.; Feig, V. R.; Lopez, J.; et al. Skin Electronics from Scalable Fabrication of an Intrinsically Stretchable Transistor Array. *Nature* **2018**, *555*, 83−88.
(10) Lipomi, D. J.; Bao, Z. Stretchable and Ultraflexible Organic Electronics. *MRS Bull.* **2017**, *42*, 93−97.
(11) Xu, J.; Wang, S.; Wang, G.-J. N.; Zhu, C.; Luo, S.; Jin, L.; Gu, X.; Chen, S.; Feig, V. R.; To, J. W. F.; et al. Highly Stretchable Polymer Semiconductor Films through the Nanoconfinement Effect. *Science* **2017**, *355*, 59−64.
(12) Oh, J. Y.; Rondeau-Gagné, S.; Chiu, Y. C.; Chortos, A.; Lissel, F.; Wang, G. J. N.; Schroeder, B. C.; Kurosawa, T.; Lopez, J.; Katsumata, T.; et al. Intrinsically Stretchable and Healable Semiconducting Polymer for Organic Transistors. *Nature* **2016**, *539*, 411−415.
(13) Xu, J.; Wu, H. C.; Zhu, C.; Ehrlich, A.; Shaw, L.; Nikolka, M.; Wang, S.; Molina-Lopez, F.; Gu, X.; Luo, S.; et al. Multi-Scale Ordering in Highly Stretchable Polymer Semiconducting Films. *Nat. Mater.* **2019**, *18*, 594−601.
(14) Gong, X.; Tong, M.; Xia, Y.; Cai, W.; Moon, J. S.; Cao, Y.; Yu, G.; Shieh, C.-L.; Nilsson, B.; Heeger, A. J. High-Detectivity Polymer Photodetectors with Spectral Response from 300 Nm to 1450 Nm. *Science* **2009**, *325*, 1665−1667.
(15) Yang, S. H.; Hsu, C. S. Liquid Crystalline Conjugated Polymers and Their Applications in Organic Electronics. *J. Polym. Sci., Part A: Polym. Chem.* **2009**, *47*, 2713−2733.
(16) Zhu, Z.; Swager, T. M. Conjugated Polymer Liquid Crystal Solutions: Control of Conformation and Alignment. *J. Am. Chem. Soc.* **2002**, *124*, 9670−9671.
(17) Kim, B. G.; Jeong, E. J.; Chung, J. W.; Seo, S.; Koo, B.; Kim, J. A Molecular Design Principle of Lyotropic Liquid-Crystalline Conjugated Polymers with Directed Alignment Capability for Plastic Electronics. *Nat. Mater.* **2013**, *12*, 659−664.
(18) Sirringhaus, H.; Tessler, N.; Friend, R. H. Integrated Optoelectronic Devices Based on Conjugated Polymers. *Science* **1998**, *280*, 1741−1744.
(19) Zhang, W.; Milner, S. T.; Gomez, E. D. Nematic Order Imposes Molecular Weight Effect on Charge Transport in Conjugated Polymers. *ACS Cent. Sci.* **2018**, *4*, 413−421.
(20) McCulloch, I.; Heeney, M.; Bailey, C.; Genevicius, K.; MacDonald, I.; Shkunov, M.; Sparrowe, D.; Tierney, S.; Wagner, R.; Zhang, W.; et al. Liquid-Crystalline Semiconducting Polymers with High Charge-Carrier Mobility. *Nat. Mater.* **2006**, *5*, 328−333.
(21) Gu, X.; Shaw, L.; Gu, K.; Toney, M. F.; Bao, Z. The Meniscus-Guided Deposition of Semiconducting Polymers. *Nat. Commun.* **2018**, *9*, No. 534.
(22) Tao, Y.; Ma, B.; Segalman, R. A. Self-Assembly of Rod-Coil Block Copolymers and Their Application in Electroluminescent Devices. *Macromolecules* **2008**, *41*, 7152−7159.
(23) Sirringhaus, H.; Wilson, R. J.; Friend, R. H.; Inbasekaran, M.; Wu, W.; Woo, E. P.; Grell, M.; Bradley, D. D. C. Mobility Enhancement in Conjugated Polymer Field-Effect Transistors through Chain Alignment in a Liquid-Crystalline Phase. *Appl. Phys. Lett.* **2000**, *77*, 406−408.
(24) Noriega, R.; Salleo, A.; Spakowitz, A. J. Chain Conformations Dictate Multiscale Charge Transport Phenomena in Disordered Semiconducting Polymers. *Proc. Natl. Acad. Sci. U.S.A.* **2013**, *110*, 16315−16320.
(25) Kuei, B.; Gomez, E. D. Chain Conformations and Phase Behavior of Conjugated Polymers. *Soft Matter* **2017**, *13*, 49−67.
(26) Vezie, M. S.; Few, S.; Meager, I.; Pieridou, G.; Dörling, B.; Ashraf, R. S.; Goñi, A. R.; Bronstein, H.; McCulloch, I.; Hayes, S. C.; et al. Exploring the Origin of High Optical Absorption in Conjugated Polymers. *Nat. Mater.* **2016**, *15*, No. 746.
(27) McCulloch, B.; Ho, V.; Hoarfrost, M.; Stanley, C.; Do, C.; Heller, W. T.; Segalman, R. A. Polymer Chain Shape of Poly(3-Alkylthiophenes) in Solution Using Small-Angle Neutron Scattering. *Macromolecules* **2013**, *46*, 1899−1907.
(28) Danielsen, S. P. O.; Davidson, E. C.; Fredrickson, G. H.; Segalman, R. A. Absence of Electrostatic Rigidity in Conjugated Polyelectrolytes with Pendant Charges. *ACS Macro Lett.* **2019**, 1147−1152.
(29) Xi, Y.; Wolf, C. M.; Pozzo, L. D. Self-Assembly of Donor-Acceptor Conjugated Polymers Induced by Miscible 'poor'' Solvents'. *Soft Matter* **2019**, *15*, 1799−1812.
(30) Newbloom, G. M.; Hoffmann, S. M.; West, A. F.; Gile, M. C.; Sista, P.; Cheung, H. K. C.; Luscombe, C. K.; Pfaendtner, J.; Pozzo, L. D. Solvatochromism and Conformational Changes in Fully Dissolved Poly(3-Alkylthiophene)S. *Langmuir* **2015**, *31*, 458−468.
(31) Reid, D. R.; Jackson, N. E.; Bourque, A. J.; Snyder, C. R.; Jones, R. L.; de Pablo, J. J. Aggregation and Solubility of a Model Conjugated Donor−Acceptor Polymer. *J. Phys. Chem. Lett.* **2018**, *9*, 4802−4807.
(32) Zheng, Y. Q.; Yao, Z. F.; Lei, T.; Dou, J. H.; Yang, C. Y.; Zou, L.; Meng, X.; Ma, W.; Wang, J. Y.; Pei, J. Unraveling the Solution-State Supramolecular Structures of Donor−Acceptor Polymers and Their Influence on Solid-State Morphology and Charge-Transport Properties. *Adv. Mater.* **2017**, *29*, No. 746.
(33) Mei, J.; Diao, Y.; Appleton, A. L.; Fang, L.; Bao, Z. Integrated Materials Design of Organic Semiconductors for Field-Effect Transistors. *J. Am. Chem. Soc.* **2013**, *135*, 6724−6746.
(34) Beaujuge, P. M.; Fr, J. M. J. Molecular Design and Ordering Effects in π-Functional Materials for Transistor and Solar Cell Applications. *J. Am. Chem. Soc.* **2011**, *133*, 20009−20029.
(35) Matthews, J. R.; Niu, W.; Tandia, A.; Wallace, A. L.; Hu, J.; Lee, W.; Giri, G.; Mannsfeld, S. C. B.; Xie, Y.; Cai, S.; et al. Scalable Synthesis of Fused Thiophene-Diketopyrrolopyrrole Semiconducting Polymers Processed from Nonchlorinated Solvents into High Performance Thin Film Transistors. *Chem. Mater.* **2013**, *25*, 782−789.
(36) Cheng, Y. J.; Yang, S. H.; Hsu, C. S. Synthesis of Conjugated Polymers for Organic Solar Cell Applications. *Chem. Rev.* **2009**, *109*, 5868−5923.
(37) Zhang, S.; Ocheje, M. U.; Huang, L.; Galuska, L.; Cao, Z.; Luo, S.; Cheng, Y.-H.; Ehlenberg, D.; Goodman, R. B.; Zhou, D.; et al. The Critical Role of Electron-Donating Thiophene Groups on the Mechanical and Thermal Properties of Donor-Acceptor Semiconducting Polymers. *Adv. Electron. Mater.* **2019**, *5*, No. 1800899.
(38) Carbone, P.; Troisi, A. Charge Diffusion in Semiconducting Polymers: Analytical Relation between Polymer Rigidity and Time Scales for Intrachain and Interchain Hopping. *J. Phys. Chem. Lett.* **2014**, *5*, 2637−2641.
(39) Adachi, T.; Brazard, J.; Ono, R. J.; Hanson, B.; Traub, M. C.; Wu, Z.-Q.; Li, Z.; Bolinger, J. C.; Ganesan, V.; Bielawski, C. W.; et al. Regioregularity and Single Polythiophene Chain Conformation. *J. Phys. Chem. Lett.* **2011**, *2*, 1400−1404.
(40) Ning, L.; Han, G.; Yi, Y. Conformational and Aggregation Properties of PffBT4T Polymers: Atomistic Insight into the Impact of Alkyl-Chain Branching Positions. *J. Mater. Chem. C* **2019**, *7*, 14198−14204.
(41) Wignall, G. D.; Melnichenko, Y. B. Recent Applications of Small-Angle Neutron Scattering in Strongly Interacting Soft Condensed Matter. *Rep. Prog. Phys.* **2005**, *68*, 1761−1810.
(42) Kyaw, A. K. K.; Wang, D. H.; Wynands, D.; Zhang, J.; Nguyen, T. Q.; Bazan, G. C.; Heeger, A. J. Improved Light Harvesting and Improved Efficiency by Insertion of an Optical Spacer (ZnO) in Solution-Processed Small-Molecule Solar Cells. *Nano Lett.* **2013**, *13*, 3796−3801.
(43) Gettinger, C. L.; Heeger, A. J.; Drake, J. M.; Pine, D. J. A Photoluminescence Study of Poly(Phenylene Vinylene) Derivatives:

https://dx.doi.org/10.1021/acs.macromol.0c02086
Macromolecules XXXX, XXX, XXX−XXX

The Effect of Intrinsic Persistence Length. *J. Chem. Phys.* **1994**, *101*, 1673−1678.
(44) McCulloch, B.; Ho, V.; Hoarfrost, M.; Stanley, C.; Do, C.; Heller, W. T.; Segalman, R. A. Polymer Chain Shape of Poly(3-Alkylthiophenes) in Solution Using Small-Angle Neutron Scattering. *Macromolecules* **2013**, *46*, 1899−1907.
(45) Hong, W. D.; Lam, C. N.; Wang, Y.; He, Y.; Sánchez-Díaz, L. E.; Do, C.; Chen, W. R. Influence of Side Chain Isomerism on the Rigidity of Poly(3-Alkylthiophenes) in Solutions Revealed by Neutron Scattering. *Phys. Chem. Chem. Phys.* **2019**, *21*, 7745−7749.
(46) Jeffries, C. M.; Graewert, M. A.; Blanchet, C. E.; Langley, D. B.; Whitten, A. E.; Svergun, D. I. Preparing Monodisperse Macromolecular Samples for Successful Biological Small-Angle X-Ray and Neutron-Scattering Experiments. *Nat. Protoc.* **2016**, *11*, 2122.
(47) Rawiso, M.; Duplessix, R.; Picot, C. Scattering Function of Polystyrene. *Macrolmolecules* **1987**, *20*, 630−648.
(48) Adamo, M.; Poulos, A. S.; Miller, R. M.; Lopez, C. G.; Martel, A.; Porcar, L.; Cabral, J. T. Rapid Contrast Matching by Microfluidic SANS. *Lab Chip* **2017**, *17*, 1559−1569.
(49) Cao, Z.; Galuska, L.; Qian, Z.; Zhang, S.; Huang, L.; Prine, N.; Li, T.; He, Y.; Hong, K.; Gu, X. The Effect of Side-Chain Branch Position on the Thermal Properties of Poly(3-Alkylthiophenes). *Polym. Chem.* **2020**, *11*, 517−526.
(50) Shao, M.; Keum, J.; Chen, J.; He, Y.; Chen, W.; Browning, J. F.; Jakowski, J.; Sumpter, B. G.; Ivanov, I. N.; Ma, Y. Z.; et al. The Isotopic Effects of Deuteration on Optoelectronic Properties of Conducting Polymers. *Nat. Commun.* **2014**, *5*, No. 3180.
(51) Grest, G. S.; Kremer, K. Molecular Dynamics Simulation for Polymers in the Presence of a Heat Bath. *Phys. Rev. A* **1986**, *33*, 3628−3631.
(52) Kremer, K.; Grest, G. S. Dynamics of Entangled Linear Polymer Melts: A Molecular-Dynamics Simulation. *J. Chem. Phys.* **1990**, *92*, 5057−5086.
(53) Murat, M.; Grest, G. S. Structure of a Grafted Polymer Brush: A Molecular Dynamics Simulation. *Macromolecules* **1989**, *22*, 4054−4059.
(54) Dünweg, B.; Kremer, K. Molecular Dynamics Simulation of a Polymer Chain in Solution. *J. Chem. Phys.* **1993**, *99*, 6983−6997.
(55) Sarapas, J. M.; Martin, T. B.; Chremos, A.; Douglas, J. F.; Beers, K. L. Bottlebrush Polymers in the Melt and Polyelectrolytes in Solution Share Common Structural Features. *Proc. Natl. Acad. Sci. U.S.A.* **2020**, *117*, 5168−5175.
(56) Zhang, S.; Alesadi, A.; Selivanova, M.; Cao, Z.; Qian, Z.; Luo, S.; Galuska, L.; Teh, C.; Ocheje, M. U.; Mason, G. T.; et al. Toward the Prediction and Control of Glass Transition Temperature for Donor−Acceptor Polymers. *Adv. Funct. Mater.* **2020**, *30*, No. 2002221.
(57) Plimpton, S. Fast Parallel Algorithms for Short-Range Molecular Dynamics. *J. Comput. Phys.* **1995**, *117*, 1−19.
(58) Humphrey, W.; Dalke, A.; Schulten, K. VMD: Visual Molecular Dynamics. *J. Mol. Graph.* **1996**, *14*, 33−38.
(59) Li, L.; Chang, D.; Arras, M. M. L.; Li, W.; Li, T.; Keum, J. K.; Bonnesen, P. V.; Peng, X.; Hong, K. Isotope Effects on the Crystallization Kinetics of Selectively Deuterated Poly(ε-Caprolactone). *J. Polym. Sci., Part B: Polym. Phys.* **2019**, *57*, 771−779.
(60) Taukeer Khan, M.; Kaur, A.; Dhawan, S. K.; Chand, S. In-Situ Growth of Cadmium Telluride Nanocrystals in Poly(3-Hexylthiophene) Matrix for Photovoltaic Application. *J. Appl. Phys.* **2011**, *110*, No. 044509.
(61) Chang, D.; Li, T.; Li, L.; Jakowski, J.; Huang, J.; Keum, J. K.; Lee, B.; Bonnesen, P. V.; Zhou, M.; Garashchuk, S.; et al. Selectively Deuterated Poly(ε-Caprolactone)s: Synthesis and Isotope Effects on the Crystal Structures and Properties. *Macromolecules* **2018**, *51*, 9393−9404.
(62) Meier, H.; Stalmach, U.; Kolshorn, H. Effective Conjugation Length and UV/Vis Spectra of Oligomers. *Acta Polym.* **1997**, *48*, 379−384.
(63) Thienpont, H.; Rikken, G. L. J. A.; Meijer, E. W.; Ten Hoeve, W.; Wynberg, H. Saturation of the Hyperpolarizability of Oligothiophenes. *Phys. Rev. Lett.* **1990**, *65*, 2141−2144.
(64) Padmanaban, G.; Ramakrishnan, S. Segmented Conjugated Polymers. *Pramana* **2003**, *61*, 425−434.
(65) Doi, M. *Introduction to Polymer Physics*; Oxford University Press, 2004.
(66) Aime, J. P.; Bargain, F.; Schott, M.; Eckhardt, H.; Miller, G. G.; Elsenbaumer, R. L. Structural Study of Doped and Undoped Polythiophene in Solution by Small-Angle Neutron Scattering. *Phys. Rev. Lett.* **1989**, *62*, 55−58.
(67) This Work Benefited from the Use of the SasView Application, Originally Developed under NSF Award DMR-0520547. SasView Contains Code Developed with Funding from the Eu- Ropean Union's Horizon 2020 Research and Innovation Programme under the SINE20. https://doi.org/www.sasview.org/.
(68) Breßler, I.; Kohlbrecher, J.; Thünemann, A. F. SASfit: A Tool for Small-Angle Scattering Data Analysis Using a Library of Analytical Expressions. *J.Appl. Cryst.* **2015**, *48*, 1587−1598.
(69) Svaneborg, C.; Pedersen, J. S. Form Factors of Block Copolymer Micelles with Excluded-Volume Interactions of the Corona Chains Determined by Monte Carlo Simulations. *Macrolmolecules* **2002**, *35*, 1028−1037.
(70) Hsu, H. P.; Paul, W.; Binder, K. Standard Definitions of Persistence Length Do Not Describe the Local "Intrinsic" Stiffness of Real Polymer Chains. *Macromolecules* **2010**, *43*, 3094−3102.
(71) Paturej, J.; Sheiko, S. S.; Panyukov, S.; Rubinstein, M. Molecular Structure of Bottlebrush Polymers in Melts. *Sci. Adv.* **2016**, *2*, No. e1601478.
(72) Sunday, D. F.; Chremos, A.; Martin, T. B.; Chang, A. B.; Burns, A. B.; Grubbs, R. H. Concentration Dependence of the Size and Symmetry of a Bottlebrush Polymer in a Good Solvent. *Macromolecules* **2020**, *53*, 7132−7140.
(73) E. Theodorakis, P.; G. Fytas, N. Molecular Dynamics Simulations of Bottle-Brush Polymers with a Flexible Backbone under Theta and Good Solvent Conditions. *Am. J. Condens. Matter Phys.* **2012**, *2*, 101−108.
(74) Zhang, W.; Gomez, E. D.; Milner, S. T. Predicting Nematic Phases of Semiflexible Polymers. *Macromolecules* **2015**, *48*, 1454−1462.
(75) Hsu, H. P.; Binder, K.; Paul, W. How to Define Variation of Physical Properties Normal to an Undulating One-Dimensional Object. *Phys. Rev. Lett.* **2009**, *103*, 1−4.
(76) Zhang, X.; Bronstein, H.; Kronemeijer, A. J.; Smith, J.; Kim, Y.; Kline, R. J.; Richter, L. J.; Anthopoulos, T. D.; Sirringhaus, H.; Song, K.; et al. Molecular Origin of High Field-Effect Mobility in an Indacenodithiophene- Benzothiadiazole Copolymer. *Nat. Commun.* **2013**, *4*, No. 2238.

https://dx.doi.org/10.1021/acs.macromol.0c02086
Macromolecules XXXX, XXX, XXX−XXX